Stem Cell Reports
Article

ISSCR

OPEN ACCESS

Argonaute 2 Is Required for Extra-embryonic Endoderm Differentiation of Mouse Embryonic Stem Cells

Richard Patryk Ngondo,[1,4] Daniel Cirera-Salinas,[1,4] Jian Yu,[1,2] Harry Wischnewski,[1] Maxime Bodak,[1,2] Sandrine Vandormael-Pournin,[3] Anna Geiselmann,[3] Rahel Wettstein,[1,2] Janina Luitz,[1] Michel Cohen-Tannoudji,[3] and Constance Ciaudo[1,*]

[1]Swiss Federal Institute of Technology Zurich, IMHS, Chair of RNAi and Genome Integrity, Zurich, Switzerland
[2]Life Science Zurich Graduate School, University of Zürich, Zurich, Switzerland
[3]Institut Pasteur, CNRS, Unité de Génétique Fonctionnelle de la Souris, UMR 3738, Department of Developmental & Stem Cell Biology, 25 rue du docteur Roux, 75015 Paris Cedex, France
[4]Co-first author
*Correspondence: cciaudo@ethz.ch
https://doi.org/10.1016/j.stemcr.2017.12.023

SUMMARY

In mouse, although four Argonaute (AGO) proteins with partly overlapping functions in small-RNA pathways exist, only *Ago2* deficiency causes embryonic lethality. To investigate the role of AGO2 during mouse early development, we generated *Ago2*-deficient mouse embryonic stem cells (mESCs) and performed a detailed characterization of their differentiation potential. *Ago2* disruption caused a global reduction of microRNAs, which resulted in the misregulation of only a limited number of transcripts. We demonstrated, both *in vivo* and *in vitro,* that AGO2 is dispensable for the embryonic germ-layer formation. However, *Ago2*-deficient mESCs showed a specific defect during conversion into extra-embryonic endoderm cells. We proved that this defect is cell autonomous and can be rescued by both a catalytically active and an inactive *Ago2,* but not by *Ago2* deprived of its RNA binding capacity or by *Ago1* overexpression. Overall, our results suggest a role for AGO2 in stem cell differentiation.

INTRODUCTION

RNA-silencing pathways play an important role in a wide range of biological processes, including regulation of animal development, cell proliferation, and differentiation (Ghildiyal and Zamore, 2009). In mammals, microRNAs (miRNAs) are the main RNA-silencing molecules and are involved in the post-transcriptional regulation of gene expression (Jonas and Izaurralde, 2015). miRNAs are about 22 nt long RNA molecules processed from longer hairpin transcripts by the consecutive cleavage of the RNase III-like enzymes DROSHA and DICER (Ha and Kim, 2014). Mature miRNAs are subsequently loaded into an Argonaute (AGO) protein to form the RNA-induced silencing complex, which leads to the destabilization or translational repression of the target transcripts. Out of the four AGO proteins (AGO1–4) that share structural similarities (Meister, 2013) and have overlapping functions in the miRNA pathway (Su et al., 2009; Wang et al., 2012a), only AGO2 possesses an endonuclease catalytic activity (Liu, 2004). In mice, the deletion of the *Ago2* gene leads to embryonic lethality, while *Ago1*, *Ago3*, and *Ago4* deletions are viable (Alisch et al., 2007; Cheloufi et al., 2010; Liu, 2004; Modzelewski et al., 2012; Morita et al., 2007; O'Carroll et al., 2007; Van Stry et al., 2012). The developmental arrest observed in *Ago2* mutant embryos occurs post-implantation and is not dependent on its catalytic activity (Cheloufi et al., 2010).

At implantation, the mouse embryo is composed of three lineages: the trophectoderm that will give rise to the placenta, the primitive endoderm (PrE) contributing to the yolk sac, and the epiblast (EPI), which will form the embryo proper (Arnold and Robertson, 2009; Rossant and Tam, 2009). The EPI and PrE are specified within the inner cell mass (ICM) at the blastocyst stage. This process is characterized by the mutually exclusive expression of lineage-specific transcription factors: NANOG in the EPI-biased cells versus GATA6 in the PrE-biased cells (Chazaud and Yamanaka, 2016). The fibroblast growth factor 4/mitogen-activated protein kinase (FGF4/MAPK) signaling pathway governs this cell-fate choice by promoting the expression of PrE genes and the repression of EPI genes within the initially homogeneous ICM (Chazaud et al., 2006; Kang et al., 2012; Nichols et al., 2009; Yamanaka et al., 2010). In this process, *Gata6* is downstream of the FGF-signaling pathway and upstream of secondary extra-embryonic endoderm (ExEn) genes such as *Gata4*, *Pdgfra*, and *Sox17* (Artus et al., 2010, 2011; Chazaud et al., 2006; Niakan et al., 2010; Plusa et al., 2008). *Gata6* mutant embryos die post-implantation and display a compromised PrE differentiation (Bessonnard et al., 2014; Koutsourakis et al., 1999; Morrisey et al., 1998; Schrode et al., 2014). *In vitro*, *Gata6* mutant mouse embryonic stem cells (mESCs) cannot induce the expression of ExEn genes and fail to establish ExEn lineage during embryoid body (EB) formation (Capo-chichi et al., 2005).

In order to investigate the roles of AGO2 in pluripotent stem cells, we generated *Ago2* knockout (*Ago2*_KO) mESCs and assessed their differentiation potential *in vitro* and

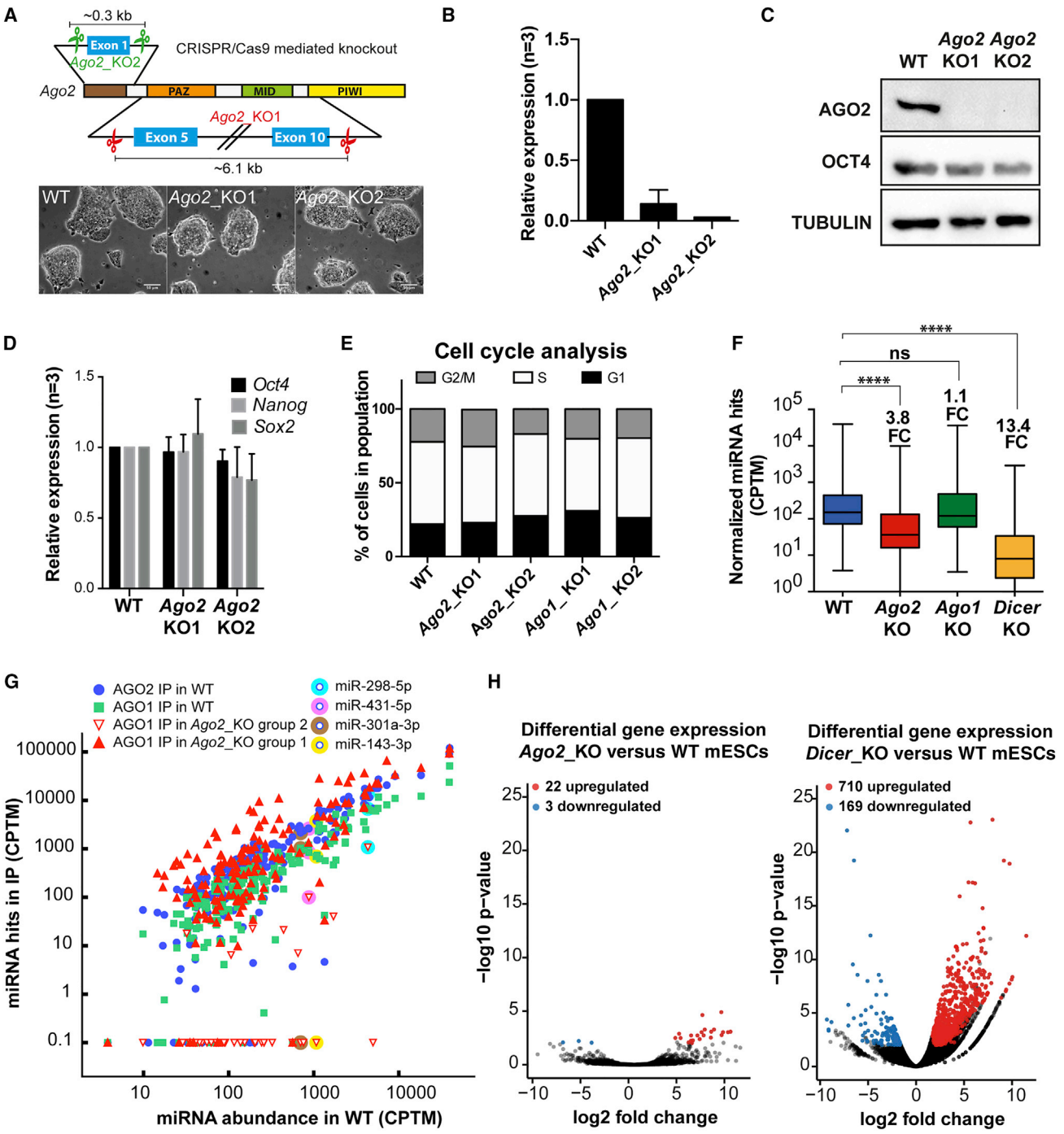

Figure 1. Characterization of *Ago2* Knockout mESCs and Impact on Gene Expression

(A) Top: schematic representation of the CRISPR/Cas9-mediated *Ago2*_KO strategy. Bottom: representative pictures of the wild-type (WT) and *Ago2*_KO mESC clones. Scale bars, 50 μm.

(B) Relative expression of *Ago2* mRNA in WT, *Ago2*_KO1, and *Ago2*_KO2 mESCs, measured by RT-qPCR. The error bars show the SD of three independent experiments.

(C) Western blot analysis of AGO2 and OCT4 protein levels in WT and *Ago2*_KO mESCs. TUBULIN is used as loading control.

(D) Relative expression of *Oct4*, *Nanog*, and *Sox2* mRNAs in WT and *Ago2*_KO cells, measured by RT-qPCR. The error bars show the SD of three independent experiments.

(legend continued on next page)

in vivo. Although *Ago2*_KO mESCs successfully differentiate toward the three embryonic germ layers, they were unable to give rise to ExEn during EB differentiation and conversion of mESCs to ExEn stem cells (XEN) (Cho et al., 2012; Kunath, 2005). The deletion of *Ago2* results in an impaired expression of GATA6 protein and ExEn genes during *in vitro* XEN conversion, leading to a cell-autonomous differentiation defect. The observed phenotype is specific to *Ago2* and overexpression of AGO1 in *Ago2*_KO mESCs does not rescue the phenotype. Finally, we demonstrate that the catalytic function of AGO2 is not required, whereas its small-RNA binding capacity is essential for the XEN conversion of *Ago2*_KO mESCs. Our findings provide insights into the understanding of AGO2 function during stem cell differentiation and identify AGO2 as a player in ExEn formation *in vitro*.

RESULTS

Generation of Argonaute Knockout Mutant mESCs

In order to assess the role of *Ago2* in mESC differentiation, we generated two independent mESC knockout clones (*Ago2*_KO1 and *Ago2*_KO2) carrying different genomic deletions generated through CRISPR/Cas9 genome editing (Doudna and Charpentier, 2014) (Figure 1A, top). Inactivation of *Ago2* was confirmed at the RNA and protein levels (Figures 1B and 1C). Both clones did not show any obvious morphological difference compared with the wild-type (WT) mESC colonies (Figure 1A, bottom) and presented no changes in expression of the core pluripotency factors *Oct4*, *Nanog,* and *Sox2* (Figures 1C and 1D).

As AGO1 is the only other AGO protein expressed in mESCs, we generated *Ago1*_KO mESCs (*Ago1*_KO1 and *Ago1*_KO2) using the same gene deletion strategy (Figures S1A–S1C). Although the alteration of the miRNA biogenesis pathway may negatively affect the cell cycle (Greve et al., 2013), we observed no significant variation in the cell cycle for *Ago2*_KO and *Ago1*_KO compared with WT mESCs (Figure 1E). Interestingly, we noticed an upregulation of AGO1 at the protein level but not at the mRNA level in *Ago2*_KO mESCs (Figures S1B and S1C), consistent with the notion that increased availability of miRNAs consecutive to the absence of AGO2 may impact the stability of AGO1 (Smibert et al., 2013).

Ago2 Knockout mESCs Show Reduced miRNA Levels with a Limited Impact on the Transcriptome

The generation of small-RNA libraries from WT, *Dicer*_KO, *Ago1*_KO, and *Ago2*_KO mESCs revealed a global reduction of the whole miRNA population (3.8-fold) in *Ago2*_KO and no significant downregulation of miRNA levels in *Ago1*_KO compared with WT mESCs (Figures 1F and S1D and Table S1). As expected, the *Dicer*_KO cells showed a strong reduction of miRNAs (13.4-fold) (Figure 1F). The expression of selected miRNAs was validated by northern blot (Figure S1E, top).

To assess whether all miRNAs could be loaded into AGO1 in the absence of AGO2, we performed immunoprecipitation of small RNAs charged in either AGO1 or AGO2 proteins in WT and *Ago2*_KO cells. While all miRNAs are bound to both proteins in WT mESCs, we observed a stronger enrichment of some miRNAs loaded in AGO1 in *Ago2*_KO (defined as group 1), whereas other miRNAs (defined as group 2) were not or were poorly loaded in AGO1 (Figure 1G). Those group 2 miRNAs were more affected by the loss of AGO2, incorporated less into AGO1, and were not detectable by northern blot in *Ago2*_KO mESCs (Figures 1G and S1E, bottom). Nevertheless, we did not detect any miRNA-specific sequence or length signatures distinguishing the two groups.

To establish the consequences of the global miRNA downregulation in *Ago2*_KO mESCs, we analyzed the transcriptome of WT and *Ago2*_KO mESCs by RNA sequencing (RNA-seq). Surprisingly, we identified only 22 genes significantly upregulated in *Ago2*_KO compared with WT mESCs, which could be potential direct miRNA targets

(E) Cell-cycle analysis of WT, *Ago2*_KO1, *Ago2*_KO2, *Ago1*_KO1, and *Ago1*_KO2. Stacked bars represent the percentage of cells in G2/M, S, or G1 phase of the cell cycle. The values were obtained from three independent experiments.

(F) Boxplots depicting the global levels of miRNAs in WT, *Ago2*_KO, *Ago1*_KO, and *Dicer*_KO mESCs measured by small-RNA-seq. The normalized miRNA reads are represented as the mean of two replicates (except for *Dicer*_KO) in counts per 10 million (CPTM). The significance (****$p < 0.0001$) was assessed using non-parametrical Mann-Whitney ranked test. The fold change (FC) relative to WT cells was calculated by comparing the mean miRNA levels in each condition.

(G) Scatterplot representing the miRNA levels in CPTM after AGO1 and AGO2 immunoprecipitation compared with WT mESCs. AGO2- and AGO1-loaded miRNAs in WT cells are represented in blue and green. The AGO1-loaded miRNAs in *Ago2*_KO mESCs from groups 1 and 2 are represented in red. Group 2 defines miRNAs 2-fold less enriched in *Ago2*_KO compared with WT mESCs. The remaining miRNAs are defined as group 1. Four miRNAs from group 2, validated by northern blot (Figure S1E), are highlighted.

(H) Volcano plots representing the differentially expressed genes in *Ago2*_KO (left) and *Dicer*_KO (right) cells compared with WT mESCs. RNA-seq data represent the mean expression of two independent biological replicates. Significantly (fold change >2 and adjusted p value <0.01) up- and downregulated genes are highlighted in red and blue, respectively.

See also Figure S1.

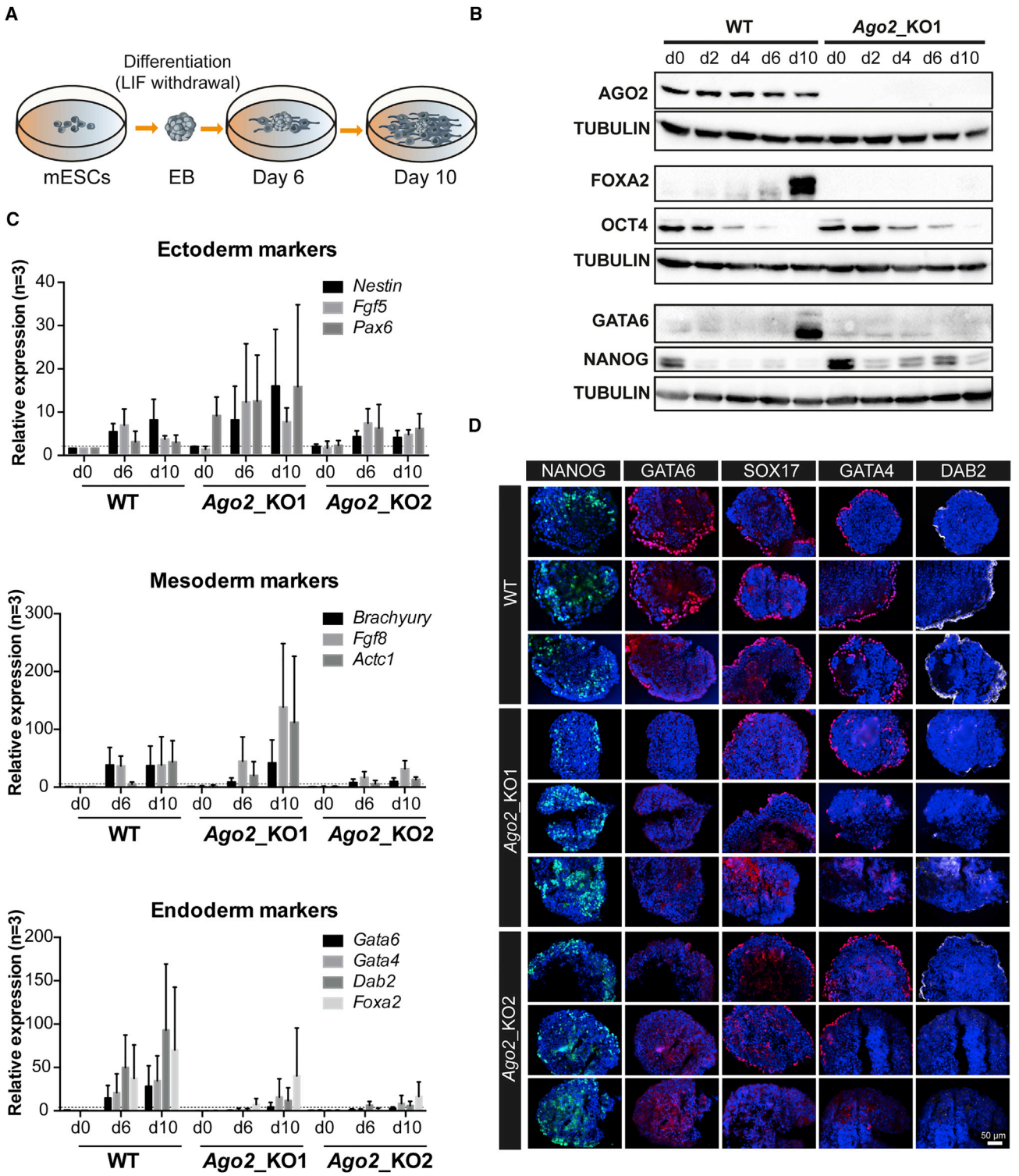

Figure 2. Embryoid Body Differentiation of *Ago2*_KO mESCs

(A) Schematic representation of the EB differentiation protocol. LIF, leukemia inhibitory factor.

(B) Western blot showing the expression of AGO2, FOXA2, OCT4, GATA6, and NANOG proteins after 0, 2, 4, 6, and 10 days of EB differentiation of WT and *Ago2*_KO1 mESCs. TUBULIN is shown as loading control.

(legend continued on next page)

(Figures 1H, left, and S1F and Table S2). For comparison, 710 transcripts were significantly upregulated in *Dicer*_KO mESCs (Figure 1H, right) (Bodak et al., 2017). Taken together, our results highlight the predominant role of AGO2 in the miRNA pathway in mESCs. Although *Ago2* deletion globally destabilizes miRNAs, it does not significantly impair the mESC gene expression patterns.

Impaired Expression of Extra-embryonic Endoderm Markers in *Ago2*_KO Embryoid Bodies

To assess the role of *Ago2* in mESC differentiation, we generated EB from *Ago2*_KO and WT mESCs and monitored the expression of different markers (Figures 2A–2C). During EB formation, mESCs differentiate into cell types derived from the three germ layers surrounded by an outer layer of ExEn. For both *Ago2*_KO and WT cells, we observed a similar downregulation of the pluripotency factor OCT4 (Figure 2B) and upregulation of ectoderm (*Nestin, Fgf5, Pax6*) and mesoderm (*Brachyury, Fgf8, Actc1*) markers (Figure 2C) over time. In contrast, the expression of *Gata6, Gata4*, and *Foxa2,* expressed in both extra-embryonic and definitive endoderm (DE), was severely impaired in *Ago2*_KO compared with WT cells (Figures 2B and 2C). Interestingly, expression of *Cxcr4, Cldn6,* and *Foxa1,* which are preferentially expressed in DE (Wang et al., 2012b), was similar in *Ago2*_KO1 and WT differentiated cells (Figure S2A). In contrast, the expression of *Dab2,* a gene preferentially expressed in ExEn, was strongly reduced in *Ago2*_KO compared with WT cells (Figure 2C), suggesting that ExEn but not DE differentiation was affected in *Ago2*-deficient cells. To confirm this observation, we used a direct differentiation protocol of mESCs toward DE (Figure S2B) (Gouon-Evans et al., 2006) and found that *Ago2_KO* and WT cells were equally competent to give rise to DE precursor cells expressing high levels of CXCR4 and c-KIT (Figures S2C and S2D). We subsequently performed immunostaining on sections of 10 day old EBs (Figure 2D). Contrary to WT EBs, having an outer epithelial layer of ExEn cells expressing GATA6, SOX17, GATA4, and DAB2, the majority of the *Ago2*_KO EBs were lacking an outer epithelial layer and showed a strongly reduced expression of GATA6, SOX17, and DAB2 (Figure 2D). A variable expression of GATA4 was still observed on the outer layer in some *Ago2*_KO EBs. Moreover, we noticed a persistent weak expression of NANOG pluripotency factor in *Ago2*_KO EBs compared with WT, by both western blot and immunofluorescence (Figures 2B and 2D). The defect in ExEn differentiation was specific for the *Ago2*_KO mESCs, as both normal expression of markers and differentiation of an outer epithelial layer were observed for *Ago1*_KO mESCs (Figures S2E and S2F). Altogether, our data show that in the absence of *Ago2*, mESCs can exit from the pluripotency state and differentiate into derivatives of the three germ layers, but are defective in the formation or the maintenance of ExEn.

Ago2-Deficient mESCs Differentiate into Embryonic Germ Layers

To further investigate whether *Ago2*_KO mESCs were able to differentiate into DE *in vivo*, we generated chimeric mice with untagged and GFP-tagged WT and *Ago2*_KO mESCs (Figures S3A and S3B). Chimeras were obtained with similar efficiency following injections of mESCs of both genotypes into C57BL/6N blastocysts (Figures 3A and S3C–S3E). Mouse ESC contribution to internal organs was monitored by simple sequence length polymorphism (SSLP) genotyping PCR on mouse tissues derived from the three embryonic germ layers: ectoderm (brain, eyes, skin), DE (thymus, lung, liver), and mesoderm (heart, spleen, kidney). We took advantage of several microsatellite repeats that are polymorphic between injected mESCs (E14 line, 129/Ola strain) and the recipient blastocyst (C57BL/6 strain) (Figures 3A, S3C, S3D, and S3F). Similar variable contribution to internal organs was observed for both WT and *Ago2*_KO mESCs. We also monitored the contribution of WT-GFP and *Ago2*_KO-GFP mESCs to the adult pancreas by fluorescence microscopy (Figure 3B). We observed a clear co-localization of GFP with insulin in beta-islet cells and with pancreatic amylase in acinar/duct cells. In addition, we performed fluorescence-activated cell sorting analysis of dissociated pancreatic cells using the FOXA2 DE marker (Figure 3C). A similar proportion of GFP-positive cells among FOXA2-positive pancreatic cells was observed in both WT and *Ago2*_KO chimeras, indicating that *Ago2*_KO-GFP mESCs contributed normally to the formation of DE-derived adult pancreatic lineages. Since FOXA2 marker showed no co-staining with immune cell markers ($CD45^+$ and CD11b) (Figure S3G), we can exclude a contribution from infiltrating immune cells of mesodermal origin to the FOXA2 and GFP double-positive

(C) Relative gene expression of ectoderm, mesoderm, and endoderm markers in WT, *Ago2*_KO1, and *Ago2*_KO2 mESCs during EB differentiation measured by RT-qPCR. The levels at day 6 (d6) and day 10 (d10) are represented relative to the levels in WT cells at day 0 (d0). Error bars represent the SD of three biological replicates. The dashed line shows levels at d0.

(D) Immunofluorescence on EB sections after 10 days of EB differentiation of WT, *Ago2*_KO1, and *Ago2*_KO2 cells. The fluorescence signal of three different sections is shown for each of the proteins: NANOG, GATA6, SOX17, GATA4, and DAB2. The nuclei are stained with Hoechst 33342. Scale bar, 50 μm.

See also Figure S2.

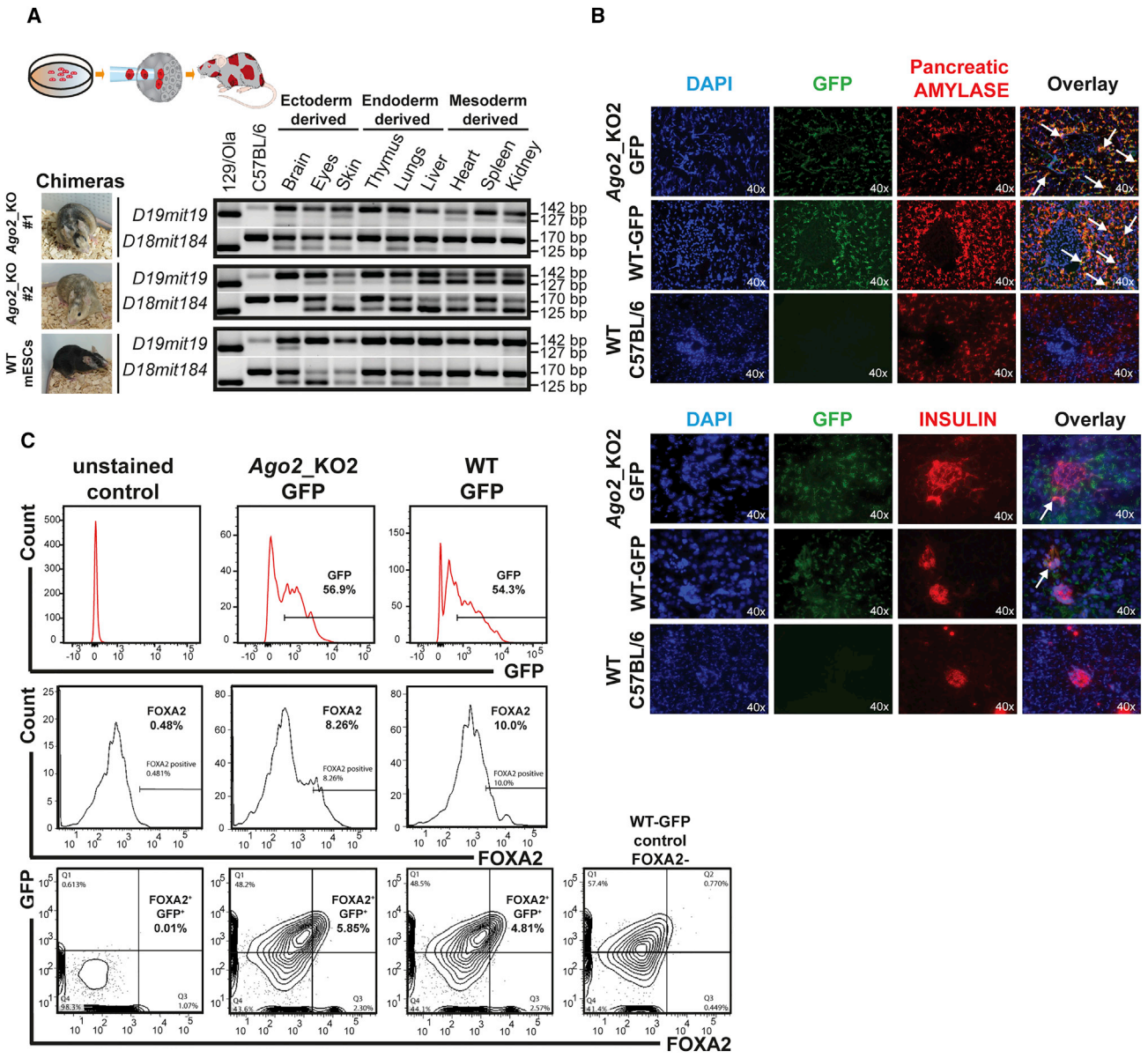

Figure 3. Generation and Analysis of Chimeric Mice

(A) SSLP PCR genotyping on DNA from tissues derived from WT and *Ago2*_KO chimeras. The contribution of the cells to the tissues was assessed following *D19mit19* and *D18mit184* microsatellite length. mESCs (129/Ola strain) were injected into recipient blastocysts (C57BL/6 strain). DNA from 129/Ola and C57BL/6 mouse strains was used as control. The pictures of the tested chimeras with various degrees of coat chimerism are presented on the left side.

(B) Immunofluorescence analysis of sections of pancreas extracted from adult *Ago2*_KO-GFP and WT-GFP chimeras. Sections from WT C57BL/6N are used as GFP-negative controls. As previously, WT and *Ago2*_KO2 mESCs expressing GFP were injected into recipient C57BL/6 blastocysts. Representative epifluorescence pictures show GFP-expressing cells, insulin-expressing pancreatic beta islets, and amylase-expressing acinar cells in non-fixed sections. Some co-expressing cells are indicated with a white arrow. Nuclei are stained with DAPI.

(C) Flow-cytometry analysis of GFP and FOXA2 definitive endoderm marker expression in pancreatic cells derived from WT-GFP and *Ago2*_KO-GFP chimeras. Pancreatic cells from WT C57BL/6 mice are used as unstained control.

See also Figure S3.

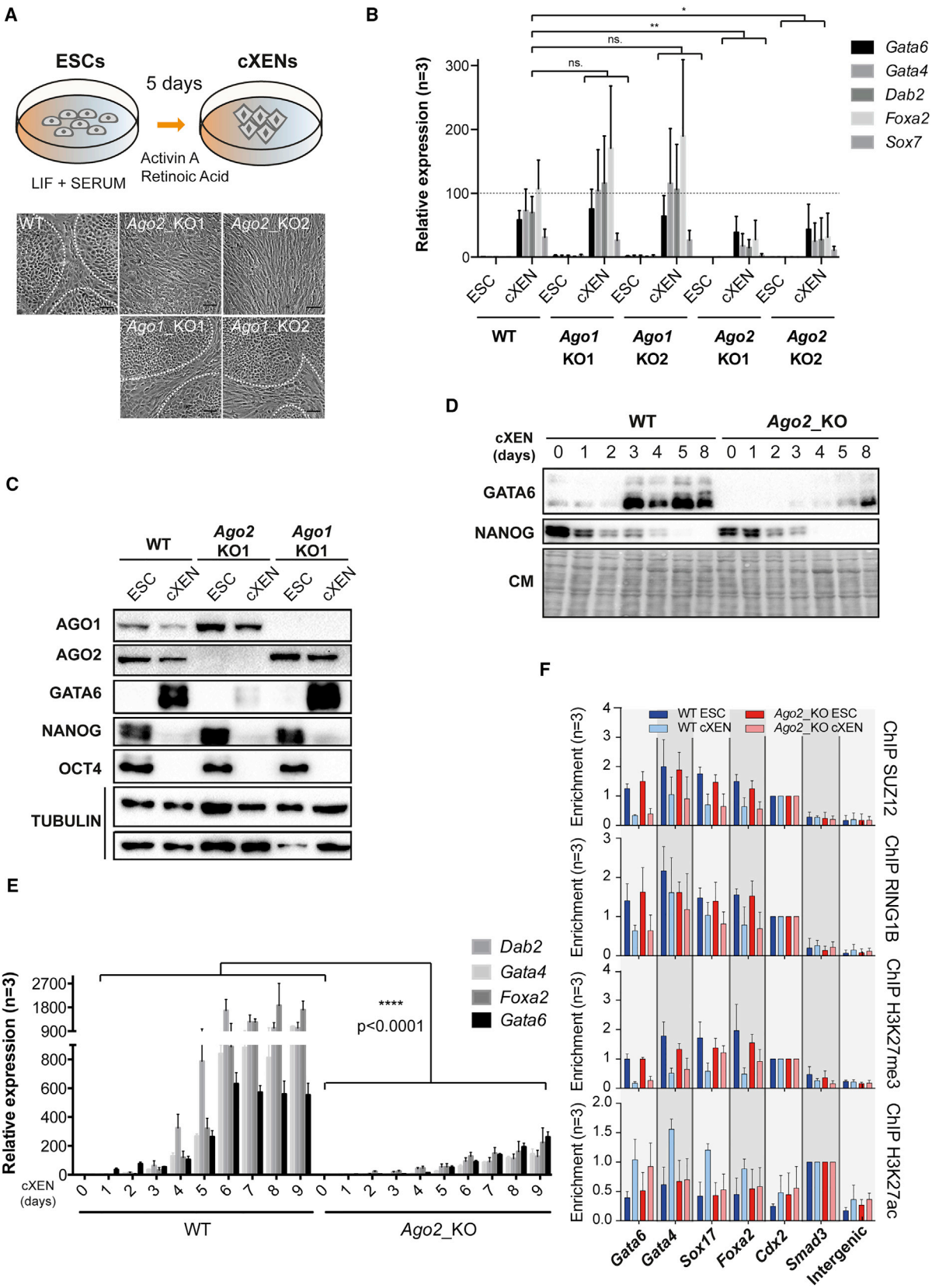

(legend on next page)

pancreatic cell population. Taken together our data show that *Ago2* is dispensable for the formation of the three embryonic germ layers including the DE.

AGO2 Is Required for ExEn Stem Cell Conversion

To better characterize the defect of *Ago2*_KO mESC differentiation into ExEn *in vitro*, we treated WT, *Ago1*_KO, and *Ago2*_KO mESCs with low doses of retinoic acid and Activin A in order to promote their differentiation into cXEN cells (Cho et al., 2012; Niakan et al., 2013) (Figure 4A). After 5 days of differentiation, we observed the formation of cXEN colonies exhibiting the characteristic epithelial-like morphology for both WT and *Ago1*_KO cells. In contrast, the two *Ago2*_KO lines predominantly showed an atypical fibroblast-like morphology (Figure 4A). The induction of secondary ExEn markers was strongly impaired in *Ago2*_KO compared with WT and *Ago1*_KO cXENs, while the expression of *Gata6* mRNA was only slightly diminished (Figure 4B). Interestingly, NANOG and OCT4 proteins were not detectable after 5 days of XEN conversion in all genotypes, whereas GATA6 protein expression was strongly reduced only in *Ago2*_KO cXENs (Figure 4C). To verify whether these observations were related to a differentiation delay, we performed a cXEN conversion time-course experiment over 8–9 days. We recapitulated previous observations (Figures 4D and 4E) and observed that *Ago2* expression was maintained all over the time course in WT cells (Figure S4A). Although GATA6 levels have been shown to be stabilized by the BMI1 in XEN cells (Lavial et al., 2012), we observed no variation of this protein in *Ago2*_KO compared with WT cXENs (Figure S4B). We next assessed the chromatin status at the promoter of *Gata6* and other secondary ExEn genes in *Ago2*_KO cells before and after cXEN conversion by chromatin immunoprecipitation (ChIP)-qPCR (Figures 4F and S4C). For both genotypes, we observed a reduced enrichment for SUZ12 and RING1B, suggesting a global de-repression of all ExEn promoters during differentiation (Rugg-Gunn et al., 2010). Strikingly, while the removal of H3K27me3 repressive marks and the deposition of H3K27ac active marks on the *Gata6* promoter were similar in both WT and *Ago2*_KO cells after conversion (Figures 4F and S4C), we observed a reduction of H3K27ac activation marks and an increase in H3K27me3 repression marks on the *Gata4, Sox17*, and *Foxa2* promoters in *Ago2*_KO compared with WT cXENs (Figures 4F and S4C). These observations suggest a post-transcriptional regulation of *Gata6* expression that leads to an impaired transcriptional induction of the secondary ExEn genes during conversion. Taken together, our data indicate that *Ago2*_KO cells fail to transcriptionally activate the proper cXEN gene expression program downstream of *Gata6*. They incorrectly engage in a different cell fate where *Gata6* post-transcriptional regulation might be mediated by multiple miRNAs (Figure S4D), suggesting a complex cell-type-dependent combinatorial regulation.

Ago2 Mutant mESCs Fail to Establish the Proper ExEn Gene Expression Program

To further explore the differentiation defect of *Ago2*_KO mESCs, we compared the expression profiles of miRNAs and mRNAs in both WT and *Ago2*_KO cXEN cells after 5 days of conversion (Tables S3 and S4). Four hundred seventy-six miRNAs were significantly misregulated between *Ago2*_KO and WT cXENs (Figures 5A and S5A). In addition,

Figure 4. cXEN Conversion of WT, *Ago2*_KO, and *Ago1*_KO Cells

(A) Schematic representation of the cXEN conversion protocol. Representative pictures of WT, *Ago2*_KO1, *Ago2*_KO2, *Ago1*_KO1, and *Ago1*_KO2 cells after 5 days of cXEN differentiation. cXEN colonies are indicated by white dashed lines. Scale bars, 50 μm.

(B) Relative gene expression of ExEn markers in WT, *Ago1*_KO, and *Ago2*_KO mESCs before (ESC) and after conversion (cXEN), measured by RT-qPCR. The error bars represent the SD of three biological replicates. The significance was assessed using a two-way ANOVA followed by Dunnett's multiple comparison for the set of ExEn markers in *Ago1*_KO and *Ago2*_KO mutants compared with the WT condition after cXEN conversion. The calculated p values are WT versus *Ago1*_KO1 ($p = 0.1655$, ns), WT versus *Ago1*_KO1 ($p = 0.1270$, ns), WT versus *Ago2*_KO1 (**$p = 0.0061$), and WT versus *Ago2*_KO2 (*$p = 0.0417$).

(C) Expression of the AGO1, AGO2, GATA6, NANOG, and OCT4 proteins before (ESC) and after (cXEN) conversion of WT, *Ago1*_KO1, and *Ago2*_KO1 cells by western blot. TUBULIN is shown as loading control for the two membranes used for blotting.

(D) Western blot analysis of GATA6 and NANOG levels at several time points during cXEN conversion of WT and *Ago2*_KO1 cells. Coomassie staining (CM) of the membrane is shown as loading control.

(E) Relative expression of ExEn markers during time series of cXEN conversion of *Ago2*_KO and WT cells, measured by RT-qPCR. The error bar represents the range of three independent experiments. For each gene the statistical significance of the variation caused by the absence of *Ago2* over the time of differentiation (two factors) was assessed using a two-way ANOVA. The p values obtained for each gene are $p < 0.0001$.

(F) ChIP-qPCR experiments on *Gata6, Gata4, Sox17,* and *Foxa2* promoters before and after cXEN conversion of WT (blue/light blue) and *Ago2*_KO (red/light red) cells. Antibodies against SUZ12, RING1B, H3K27me3, and H3K27ac were used. The enrichment was calculated compared with a repressed (*Cdx2*) and an active (*Smad3*) promoter. An intergenic region was used as negative control. The error bars correspond to the SD of three independent experiments.

See also Figure S4.

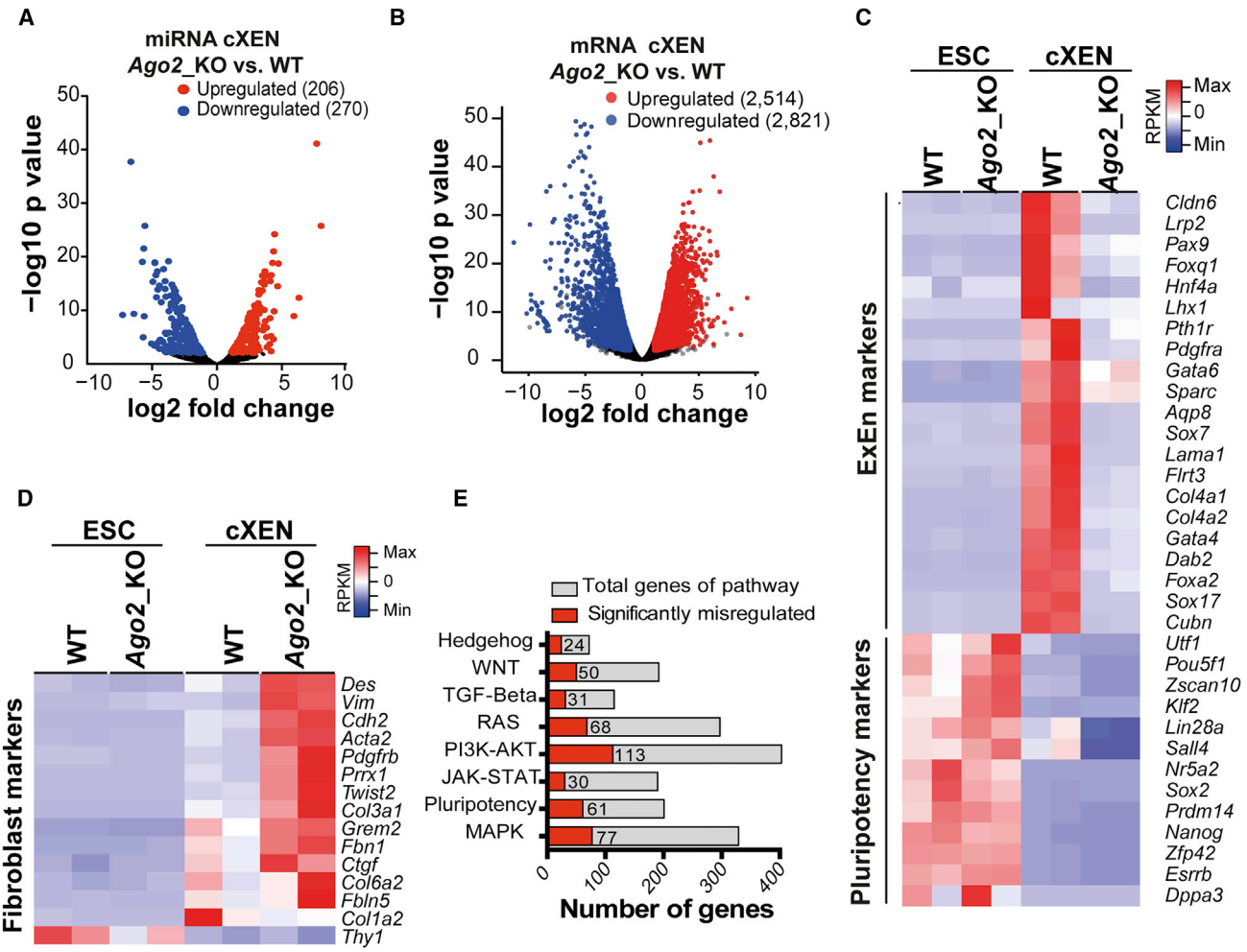

Figure 5. The Transcriptome of Aberrantly Converted *Ago2*_KO mESCs Is Distinct from that of WT cXEN

(A) Volcano plot of differentially expressed miRNAs in *Ago2*_KO compared with WT cXENs. Data are represented as the mean expression of two independent biological replicates. Significantly (2-fold change and adjusted p value < 0.01) up- and downregulated genes are highlighted in red and blue, respectively.

(B–D) Volcano plot representing the differentially expressed genes in *Ago2*_KO cells compared with WT cells after cXEN conversion (B). Data are represented as the mean expression of two independent biological replicates. Significantly (2-fold change and adjusted p value <0.01) up- and downregulated genes are highlighted in red and blue, respectively. Heatmaps depicting the expression of (C) ExEn and pluripotency markers and (D) fibroblast-related genes in *Ago2*_KO compared with WT mESCs after cXEN conversion. Two replicates are represented before (ESC) and after differentiation (cXEN). The expression levels are represented as RPKM values (reads per kilobase of transcript per million reads mapped).

(E) Bar graph representing the proportion of genes significantly misregulated in *Ago2*_KO compared with WT cells after 5 days of cXEN conversion. The represented genes are related to mESC-relevant signaling pathways. The gene list was extracted from the KEGG database (Hedgehog, WNT, TGF-beta, RAS, PI3K-AKT, JAK-STAT, MAPK, and pluripotency).

See also Figure S5.

20% of the transcripts were misregulated: 2,514 genes were significantly up- and 2,821 downregulated in *Ago2*_KO compared with WT cXENs (Figure 5B). In accordance with our previous results (Figure 4C), pluripotency markers were strongly downregulated in both WT and *Ago2*_KO cXENs, while ExEn markers were highly induced only in WT cXENs (Figure 5C). Although both mesodermal and trophectodermal markers were not induced in *Ago2*_KO cXENs, we noted an induction of mesenchymal markers, ectodermal, and fibroblast-related markers (Figures 5D and S5B). This highly divergent gene expression profile is also translated at the level of several signaling pathways such as WNT, TGF-beta, MAPK, or HEDGEHOG pathways (Figures 5E and S5C and Table S5), critical for regulation

of the cell-fate choice during early development (Frum and Ralston, 2015). Collectively our data indicate that *Ago2*_KO mESCs do not adopt an ExEn identity and differentiate into an undefined fibroblast-like cell type (Figures 4A and 5D).

*Ago2*_KO cXEN Differentiation Failure Is Cell Autonomous

In vivo, the establishment of ExEn is driven by FGF4, which is secreted by EPI-biased cells (Kang et al., 2012). Addition of FGF4 to the conversion medium of *Ago2*_KO mESCs did not rescue GATA6 protein level, nor the expression of ExEn markers (Figures 6C and S6B), neither the formation of XEN colonies (Figure S6C). Similarly, co-culture of *Ago2*_KO mESCs with GFP-labeled WT mESCs did not rescue their differentiation defects as shown by the absence of cXEN colony formation (Figure 6A) or expression of the endoderm protein FOXA2 for *Ago2*-deficient GFP-negative cells (Figures 6B and S6A). These data demonstrate that the differentiation defects of *Ago2*_KO mESCs are cell autonomous.

FGF/ERK Pathway Correctly Regulates NANOG Expression in *Ago2*_KO mESCs

Similar to WT cXEN, *Ago2*_KO cells expressed the *Fgfr2* receptor and downregulated the expression of *Fgf4* and *Nanog* mRNAs after cXEN conversion (Figure S6D), indicating that the cells normally initiate their differentiation program. Therefore, we reasoned that the defect could be related to the FGF/ERK signaling cascade. Consequently, we verified the functionality of this pathway by treating WT and *Ago2*_KO mESCs with two FGF receptor inhibitors (AZD4547; PD173074) and one MEK inhibitor (PD0325901) (Figure S6E). Phosphorylation of ERK was strongly reduced in the presence of the inhibitors and correlated with an upregulation of the NANOG protein in both WT and *Ago2*_KO mESCs. Conversely, the addition of FGF4 slightly reduced NANOG levels (Figure S6E). Notably, we observed a different response to the FGF/ERK inhibitors in the *Ago2*_KO compared with WT cells during the conversion to cXEN, as NANOG was downregulated even though the FGF/ERK signaling pathway was inhibited (Figure S6F). Taken together these experiments demonstrate that although the FGF/ERK pathway correctly regulates NANOG expression in *Ago2*_KO mESCs, its inhibition fails to maintain pluripotency under differentiation culture conditions as it does for WT mESCs.

*Ago2*_KO cXEN Differentiation Failure Is Bypassed by GATA6 Overexpression

It has been shown that GATA6 overexpression alone is sufficient to reprogram mESCs into XEN cells (Shimosato et al., 2007). Therefore, we generated mESC WT and *Ago2*_KO clones expressing GATA6 in an inducible manner. After 3 days of induction, we observed the formation of XEN-like colonies and high expression of ExEn markers in both WT-GATA6 and *Ago2*_KO-GATA6 cells (Figures 6D and S6G). Therefore, GATA6 expression is sufficient to induce XEN conversion in *Ago2*_KO mESCs, bypassing the misregulation observed in the context of XEN conversion. Taken together our data show that the XEN conversion impairment of *Ago2*-deficient mESCs is cell autonomous and can be rescued by exogenous GATA6 expression.

The AGO2 Small-RNA Binding Capacity Is Required during XEN Conversion

Finally, we performed rescue experiments by ectopically expressing inducible hemagglutinin (HA)-tagged WT (HA-AGO2), catalytic mutant D699A (CATmut) (O'Carroll et al., 2007), and small-RNA-binding mutant Y311A/Y312A (RNAmut) (Gao et al., 2014) *Ago2* cDNA in *Ago2*_KO1 mESCs (Figure 7A, top). After 5 days of induction, we observed a strong restoration of AGO2 protein levels with the CATmut *Ago2* transgene and a weaker but comparable restoration with both the HA-tagged WT *Ago2* and the RNAmut *Ago2* transgenes (Figure 7A). During cXEN conversion, induction of the HA-AGO2 and CATmut effectively rescued the impaired expression of ExEn markers (Figure 7B). Moreover, the expression level of groups 1 and 2 miRNAs, as well as the formation of cXEN colonies, was restored, despite the lower level of AGO2 protein in HA-AGO2 compared with WT mESCs (Figures 7A, 7C, and 7D). In contrast, the RNAmut transgene expression did not induce any significant change in ExEn markers nor miRNA stabilization and the cells presented a fibroblast-like morphology similar to that of the *Ago2*_KO cells after conversion (Figures 7B–7D).

To assess if AGO1 might rescue *Ago2* phenotypes, we overexpressed AGO1 in *Ago2*_KO mESCs (Figures 7E and S7A). No significant induction of ExEn markers and no formation of XEN-like colonies were observed in *Ago2*_KO-AGO1 cells after cXEN differentiation (Figures 7F and 7G). Nevertheless, we observed a global restoration of the expression of both groups of miRNAs before cXEN conversion (Figures S7B–S7D and Table S6). The functionality of these restored miRNAs was also validated by measuring the level of potential miRNA targets, upregulated in *Ago2*_KO cells (Figures S1F and S7E). Taken together, our results show that AGO2 but not AGO1 is required for the correct induction of the ExEn markers and the formation of cXEN colonies. We demonstrated that AGO2 small-RNA binding capacity but not its catalytic activity is essential for this differentiation process. Moreover, AGO1 overexpression and miRNA restoration is not sufficient to rescue *Ago2*_KO XEN conversion defect.

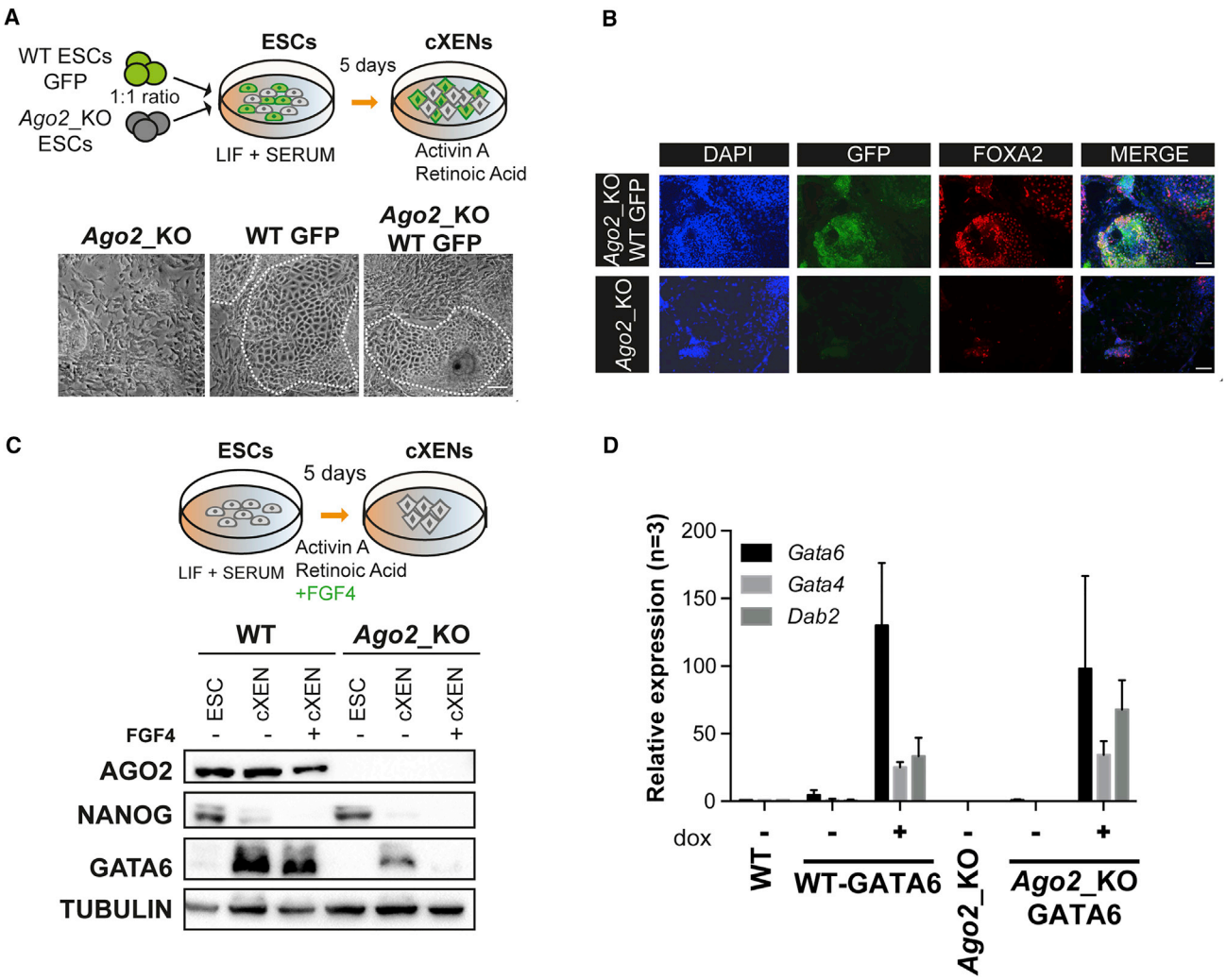

Figure 6. cXEN Conversion Defect of *Ago2*_KO mESCs Is Cell Autonomous

(A) Schematic representation of the cXEN differentiation of WT and *Ago2*_KO cells co-cultured in a 1:1 ratio. The WT cells are GFP positive and *Ago2*_KO cells are GFP negative. Representative pictures of the *Ago2*_KO, WT-GFP, and WT-GFP/*Ago2*_KO cXEN cell conversion are shown. cXEN colonies are indicated by white dashed lines. Scale bar, 50 μm.

(B) Immunofluorescence of WT-GFP/*Ago2*_KO co-cultured cells after cXEN conversion. Representative picture of GFP and FOXA2 co-stained sample is shown. The XENs that appear in the co-cultures are GFP positive. Nuclei are stained with DAPI. *Ago2*_KO cXEN converted cells are shown as negative control. Scale bars, 50 μm.

(C) WT and *Ago2*_KO mESCs were converted to cXEN in the presence of 500 ng/mL FGF4 growth factor + 1 μg/mL heparin. Schematic representation of the experiment is presented. Levels of AGO2, NANOG, and GATA6 in the different conditions after conversion are shown. TUBULIN levels are shown as loading control. Undifferentiated cells (ESC) are used as controls.

(D) RT-qPCR quantification of ExEn markers (*Gata6, Gata4,* and *Dab2*) in WT-GATA6 and *Ago2*_KO-GATA6 mESCs, expressing exogenous inducible GATA6, cultured in LIF/serum conditions for 3 days with or without the addition of doxycycline. The error bar represents the SD of three replicate experiments.

See also Figure S6.

DISCUSSION

In this study, we used mESCs and their differentiation derivatives as a model system to investigate the underlying causes of the post-implantation lethality of the *Ago2* mutant mouse embryos. By generating *Ago1*- and *Ago2*-deficient mutant mESCs in the same genetic background, we demonstrated that the deletion of either one of these two genes had no significant effect on mESCs, cell cycle, and self-renewal. Deletion of *Ago2* compromised miRNA

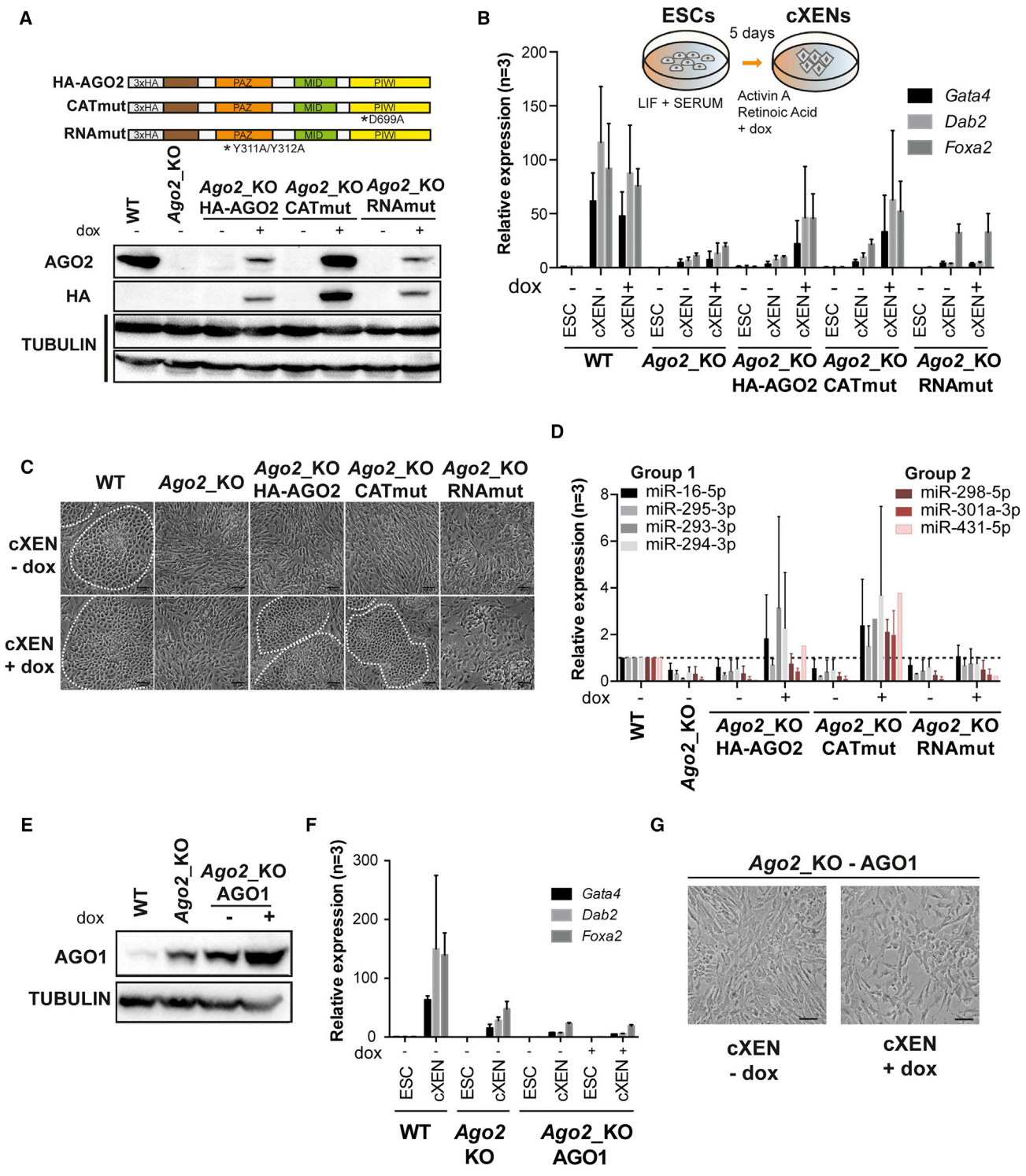

Figure 7. XEN Conversion of mESCs Requires the Small-RNA Binding Capacity of AGO2

(A) Schematic representation of the inducible constructs used for the ectopic expression of HA-tagged AGO2, catalytic AGO2 mutant (CATmut), and small-RNA-binding deficient PAZ domain AGO2 mutant (RNAmut) in *Ago2*_KO1 mESCs. Expression of the AGO2 constructs after 5 days of induction with doxycycline (dox) is shown. TUBULIN is used as loading control.

(B) cXEN conversion of *Ago2*_KO complemented mutants with or without doxycycline. The relative expression of ExEn markers was measured by RT-qPCR before (ESC) and after conversion (cXEN). The error bars represent the SD of three independent experiments.

(legend continued on next page)

levels, with a weak impact on the transcriptome, indicating its preponderant role in the miRNA pathway in mESCs and potential compensatory function of the AGO1 protein, in line with previous observations (Su et al., 2009). Indeed, the upregulated AGO1 stabilizes the steady-state miRNA level in *Ago2*_KO mESCs. This observation is also in accordance with the previously described correlation between AGO abundance and miRNA availability (Martinez and Gregory, 2013; O'Carroll et al., 2007; Wang et al., 2012a; Winter and Diederichs, 2014). Notably, miRNAs moderately (group 1) or strongly affected (group 2) by *Ago2* deletion were broadly rescued by AGO1 ectopic overexpression, demonstrating a functional overlap of the two AGO proteins in miRNA loading and stabilization in mESCs.

The miRNA levels have been shown to be important for embryonic development (Greve et al., 2013). Indeed, *Dicer* mutant embryos deprived of miRNAs die after implantation at 6.5 dpp (Bernstein et al., 2003) and *Dicer*_KO mESCs can be maintained *in vitro* but cannot exit pluripotency (Bodak et al., 2017). The *in vitro* differentiation of *Ago2*_KO mESCs revealed that even with reduced miRNA levels, the cells effectively differentiate toward ectodermal, mesodermal, and DE lineages. The successful generation of chimeric mice using both *Ago2*_KO mESC clones demonstrated that *Ago2* is dispensable for the post-implantation differentiation processes of the embryo. Using a cXEN conversion protocol, we proved that AGO2 is required for ExEn differentiation. Indeed, our study revealed a severe *in vitro* conversion defect of *Ago2*_KO mESCs toward XEN cells. The requirement of *Ago2* for the ExEn cell-fate choice is relevant *in vivo*, as it is expressed from the oocyte to the blastocyst stage (Lykke-Andersen et al., 2008; Park et al., 2015; Wu et al., 2016) and has been shown to be present both in embryonic and in extra-embryonic tissues (Cheloufi et al., 2010) at embryonic day E9.5. In previous *in vivo* studies, *Ago2* mutant mice were generated using insertional mutations after exon 12, after exons 3–6 (Alisch et al., 2007; Liu, 2004), or after exon 1 (Morita et al., 2007). The three studies observed an early embryonic lethality phenotype and described a developmental arrest ranging from implantation to mid-gestation. Although placenta defects have been shown to contribute to the embryonic lethality of *Ago2*-deficient embryos (Cheloufi et al., 2010), the cell-autonomous ExEn differentiation defects that we observed *in vitro* may also contribute to their *in vivo* developmental defects. Further, *in vivo* studies are required to clarify the essential role of AGO2 in PrE formation and differentiation during early development.

We demonstrated that the cXEN conversion of mESCs requires AGO2 small-RNA binding capacity but not its catalytic activity, suggesting that AGO2 loaded with a small-RNA molecule may be functionally required for this process or for the stabilization of the AGO2 protein itself. Interestingly, our experimental data indicate that the global level of miRNAs is not critical for ExEn differentiation, as its restoration by AGO1 ectopic overexpression does not rescue the *Ago2*_KO conversion defect. A previous study analyzed the miRNA content of cells derived from extra-embryonic tissues and highlighted their importance using *Dicer*_KO mutants (Spruce et al., 2010), in which AGO2 is per se downregulated due to the lack of miRNAs (Smibert et al., 2013), making it impossible to dissociate both phenotypes. Our findings point toward the presence of either some AGO2-specific small RNAs or non-canonical AGO2-specific functions during the conversion process. Furthermore, AGO2 subcellular localization may also be altered when the protein has impaired small-RNA loading (Nishi et al., 2015; Schraivogel et al., 2015) and in turn be responsible for the differentiation defect.

The considerable variation of gene expression profiles and morphology between *Ago2*_KO and WT cXENs indicates that *Ago2*_KO cells differentiate into a fibroblast-like cell fate expressing mesenchymal markers instead of epithelial markers, normally expressed by XEN cells (Brown et al., 2010). This impaired differentiation of *Ago2*_KO cells into a different cell lineage is also illustrated by their inconsistent response to the FGF/ERK pathway inhibitors on NANOG and GATA6 expression (Figures S6E and S6F). Although they exit pluripotency during conversion, *Ago2*_KO cells fail to properly express GATA6

(C) Representative pictures of the WT, *Ago2*_KO, and the complemented mutant (HA-AGO2, CATmut, and RNAmut) cells after 5 days of cXEN conversion with (+dox) or without (−dox) induction with doxycycline. cXEN colonies are indicated by white dashed lines. Scale bars, 50 μm.

(D) Relative expression of miRNAs of group 1 and group 2 in the complemented mutants before and after 5 days of doxycycline, measured by RT-qPCR. The error bars correspond to the SD of three independent experiments. The dashed line represents miRNA levels in WT cells.

(E) Western blot showing the inducible overexpression of AGO1 in stably transfected *Ago2*_KO cells (clone *Ago2*_KO-AGO1-A). The cells were induced 5 days with doxycycline. TUBULIN is used as loading control.

(F) cXEN conversion of *Ago2*_KO-AGO1-A cells with or without doxycycline. The relative expression of ExEn markers was measured by RT-qPCR before (ESC) and after conversion (cXEN). The error bars represent the SD of three independent experiments.

(G) Representative pictures of the *Ago2*_KO cells overexpressing AGO1 (*Ago2*_KO-AGO1-A and *Ago2*_KO-AGO1-B) after 5 days of cXEN conversion with (+dox) or without (−dox) induction with doxycycline. Scale bars, 50 μm.

See also Figure S7.

protein levels and consequently to activate the ExEn gene expression program downstream of GATA6. Importantly, we were able to bypass this defective regulation by ectopically expressing *Gata6* cDNA deprived of its 3′ UTR in *Ago2*_KO cells. *Ago2*_KO fibroblast-like cells have distinctive mRNA and miRNA expression profiles compared with WT XEN cells. Some of the upregulated miRNAs are loaded into AGO1 and can target the *Gata6* 3′ UTR, potentially explaining the downregulation of GATA6 protein. Alternatively, GATA6 could be destabilized in *Ago2*_KO cells due to the downregulation of an unknown cofactor, which would specifically stabilize GATA6 by preventing its degradation, like BMI1 in fully differentiated XEN cells (Lavial et al., 2012).

Finally, the role of AGO2 in XEN differentiation might also be relevant for the de-differentiation or reprogramming of somatic cells, as it has been recently demonstrated that an intermediary XEN-like state is essential for chemical generation of induced pluripotent stem cells (Zhao et al., 2015). Interestingly, our study shows that AGO2 is specifically required for the induction of XEN cell fate from mESCs, which underlines the importance of a specific RNAi pathway factor in a directed differentiation process.

EXPERIMENTAL PROCEDURES

Chimeric Mice Generation

Blastocyst micro-injections were performed at the EPIC transgenic facility (ETH, Zurich). For details see the Supplemental Experimental Procedures. All experiments were conducted according to Swiss law of animal protection and with the approval of the local institutional animal care committees (licence nos. 106/2013 and ZH123/16).

mESC Culture

The E14 mESC line (129/Ola background) was used and cultured as described previously (Bodak et al., 2017). If required, the medium was supplemented with 1 μg/mL doxycycline, 1 μM retinoic acid, 2 μM PD0325901, 0.1 μM PD173074, 1 μM AZD4547, or 500 ng/mL FGF4 + 1 μg/mL heparin.

CRISPR/Cas9-Mediated Gene Knockout

The *Ago2*_KO and *Ago1*_KO cell lines were generated using a paired CRISPR/CAS9 strategy on WT E14 mESCs as described previously (Wettstein et al., 2016).

cXEN Conversion of mESCs

The cXEN conversion was performed as described in Niakan et al. (2013).

mRNA and miRNA Expression Analysis

The mRNA and miRNA extraction and quantification were performed as described in Cirera-Salinas et al. (2017).

Cross-Linked Immunoprecipitation of AGO1/AGO2-Bound Small RNAs

The RNA immunoprecipitation was performed as described in Selth et al. (2011). The pulled-down small RNAs were analyzed by deep sequencing.

ACCESSION NUMBERS

The accession numbers for all the RNA-seq data reported in this paper are GEO: GSE78971 and GSE80454.

SUPPLEMENTAL INFORMATION

Supplemental Information includes Supplemental Experimental Procedures, seven figures, and six tables and can be found with this article online at https://doi.org/10.1016/j.stemcr.2017.12.023.

AUTHOR CONTRIBUTIONS

R.P.N. and C.C. conceived and performed experiments, interpreted the data, and wrote the manuscript with inputs from M.C.-T.; D.C.-S. performed most of the experiments for the revision of the manuscript; M.B., R.W., J.L., A.G., H.W., and S.V.-P. contributed to experiments; J.Y. and R.P.N. performed bioinformatics analysis; M.C.-T. performed experiments and provided expertise. C.C. supervised the study and secured funding.

ACKNOWLEDGMENTS

We are grateful to the ETH Phenomics Center (EPIC) for the blastocyst injections. We are thankful to Professor A. Wutz and Drs. T. Beyer, E. Girardi, S. Bessonnard, and J. Artus for helpful discussions and critical reading of the manuscript. We thank Dr. R. Freiman for single-cell sorting. We acknowledge the Functional Genomics Center Zurich (FGCZ) for technical support. We thank Dr. D. O'Carroll for the gift of *Ago2* plasmids and all the Ciaudo lab members for their help and assistance. This work was supported by a Swiss National Science Foundation grant (31003A_153220), the Helmut Horten Stiftung foundation to C.C., and the Agence Nationale de la Recherche (ANR-10-LABX-73-01 REVIVE and ANR-14CE11-0017 PrEpiSpec) to M.C.-T. D.C.-S. is supported by a post-doctoral fellowship from the Peter and Traudl Foundation. H.W. is supported by the NCCR RNA & Disease, funded by the Swiss National Science Foundation. M.B. is supported by a PhD fellowship from the ETH-Z foundation (ETH-21 13-1). J.Y. is supported by a PhD fellowship from the ETH-Z foundation (ETH-05 14-3). The authors declare no financial or non-financial competing interests.

Received: August 25, 2016
Revised: December 28, 2017
Accepted: December 28, 2017
Published: January 25, 2018

REFERENCES

Alisch, R.S., Jin, P., Epstein, M., Caspary, T., and Warren, S.T. (2007). Argonaute2 is essential for mammalian gastrulation and proper mesoderm formation. PLoS Genet. *3*, e227.

Arnold, S.J., and Robertson, E.J. (2009). Making a commitment: cell lineage allocation and axis patterning in the early mouse embryo. Nat. Rev. Mol. Cell Biol. *10*, 91–103.

Artus, J., Panthier, J.J., and Hadjantonakis, A.K. (2010). A role for PDGF signaling in expansion of the extra-embryonic endoderm lineage of the mouse blastocyst. Development *137*, 3361–3372.

Artus, J., Piliszek, A., and Hadjantonakis, A.-K. (2011). The primitive endoderm lineage of the mouse blastocyst: sequential transcription factor activation and regulation of differentiation by Sox17. Dev. Biol. *350*, 393–404.

Bernstein, E., Kim, S.Y., Carmell, M.A., Murchison, E.P., Alcorn, H., Li, M.Z., Mills, A.A., Elledge, S.J., Anderson, K.V., and Hannon, G.J. (2003). Dicer is essential for mouse development. Nat. Genet. *35*, 215–217.

Bessonnard, S., De Mot, L., Gonze, D., Barriol, M., Dennis, C., Goldbeter, A., Dupont, G., and Chazaud, C. (2014). Gata6, Nanog and Erk signaling control cell fate in the inner cell mass through a tristable regulatory network. Development *141*, 3637–3648.

Bodak, M., Cirera-Salinas, D., Yu, J., Ngondo, R.P., and Ciaudo, C. (2017). Dicer, a new regulator of pluripotency exit and LINE-1 elements in mouse embryonic stem cells. FEBS Open Bio *7*, 204–220.

Brown, K., Legros, S., Artus, J., Doss, M.X., Khanin, R., Hadjantonakis, A.K., and Foley, A. (2010). A comparative analysis of extra-embryonic endoderm cell lines. PLoS One *5*, e12016.

Capo-chichi, C.D., Rula, M.E., Smedberg, J.L., Vanderveer, L., Parmacek, M.S., Morrisey, E.E., Godwin, A.K., and Xu, X.-X. (2005). Perception of differentiation cues by GATA factors in primitive endoderm lineage determination of mouse embryonic stem cells. Dev. Biol. *286*, 574–586.

Chazaud, C., and Yamanaka, Y. (2016). Lineage specification in the mouse preimplantation embryo. Development *143*, 1063–1074.

Chazaud, C., Yamanaka, Y., Pawson, T., and Rossant, J. (2006). Early lineage segregation between epiblast and primitive endoderm in mouse blastocysts through the Grb2-MAPK pathway. Dev. Cell *10*, 615–624.

Cheloufi, S., Dos Santos, C.O., Chong, M.M., and Hannon, G.J. (2010). A dicer-independent miRNA biogenesis pathway that requires Ago catalysis. Nature *465*, 584–589.

Cho, L.T.Y., Wamaitha, S.E., Tsai, I.J., Artus, J., Sherwood, R.I., Pedersen, R.A., Hadjantonakis, A.K., and Niakan, K.K. (2012). Conversion from mouse embryonic to extra-embryonic endoderm stem cells reveals distinct differentiation capacities of pluripotent stem cell states. Development *139*, 2866–2877.

Cirera-Salinas, D., Yu, J., Bodak, M., Ngondo, R.P., Herbert, K.M., and Ciaudo, C. (2017). Noncanonical function of DGCR8 controls mESC exit from pluripotency. J. Cell Biol. *216*, 355–366.

Doudna, J.A., and Charpentier, E. (2014). The new frontier of genome engineering with CRISPR-Cas9. Science *346*, 1258096.

Frum, T., and Ralston, A. (2015). Cell signaling and transcription factors regulating cell fate during formation of the mouse blastocyst. Trends Genet. *31*, 402–410.

Gao, M., Wei, W., Li, M.M., Wu, Y.S., Ba, Z., Jin, K.X., Li, M.M., Liao, Y.Q., Adhikari, S., Chong, Z., et al. (2014). Ago2 facilitates Rad51 recruitment and DNA double-strand break repair by homologous recombination. Cell Res. *24*, 532–541.

Ghildiyal, M., and Zamore, P.D. (2009). Small silencing RNAs: an expanding universe. Nat. Rev. Genet. *10*, 94–108.

Gouon-Evans, V., Boussemart, L., Gadue, P., Nierhoff, D., Koehler, C.I., Kubo, A., Shafritz, D.A., and Keller, G. (2006). BMP-4 is required for hepatic specification of mouse embryonic stem cell-derived definitive endoderm. Nat. Biotechnol. *24*, 1402–1411.

Greve, T.S., Judson, R.L., and Blelloch, R. (2013). microRNA control of mouse and human pluripotent stem cell behavior. Annu. Rev. Cell Dev. Biol. *29*, 213–239.

Ha, M., and Kim, V.N. (2014). Regulation of microRNA biogenesis. Nat. Rev. Mol. Cell Biol. *15*, 509–524.

Jonas, S., and Izaurralde, E. (2015). Towards a molecular understanding of microRNA-mediated gene silencing. Nat. Rev. Genet. *16*, 421–433.

Kang, M., Piliszek, A., Artus, J., and Hadjantonakis, A.K. (2012). FGF4 is required for lineage restriction and salt-and-pepper distribution of primitive endoderm factors but not their initial expression in the mouse. Development *140*, 267–279.

Koutsourakis, M., Langeveld, A., Patient, R., Beddington, R., and Grosveld, F. (1999). The transcription factor GATA6 is essential for early extraembryonic development. Development *126*, 723–732.

Kunath, T. (2005). Imprinted X-inactivation in extra-embryonic endoderm cell lines from mouse blastocysts. Development *132*, 1649–1661.

Lavial, F., Bessonnard, S., Ohnishi, Y., Tsumura, A., Chandrashekran, A., Fenwick, M.A., Tomaz, R.A., Hosokawa, H., Nakayama, T., Chambers, I., et al. (2012). Bmi1 facilitates primitive endoderm formation by stabilizing Gata6 during early mouse development. Genes Dev. *26*, 1445–1458.

Liu, J. (2004). Argonaute2 is the catalytic engine of mammalian RNAi. Science *305*, 1437–1441.

Lykke-Andersen, K., Gilchrist, M.J., Grabarek, J.B., Das, P., Miska, E., and Zernicka-Goetz, M. (2008). Maternal Argonaute 2 is essential for early mouse development at the maternal-zygotic transition. Mol. Biol. Cell *19*, 4383–4392.

Martinez, N.J., and Gregory, R.I. (2013). Argonaute2 expression is post-transcriptionally coupled to microRNA abundance. RNA *19*, 605–612.

Meister, G. (2013). Argonaute proteins: functional insights and emerging roles. Nat. Rev. Genet. *14*, 447–459.

Modzelewski, A.J., Holmes, R.J., Hilz, S., Grimson, A., and Cohen, P.E. (2012). AGO4 regulates entry into meiosis and influences silencing of sex chromosomes in the male mouse germline. Dev. Cell *23*, 251–264.

Morita, S., Horii, T., Kimura, M., Goto, Y., Ochiya, T., and Hatada, I. (2007). One Argonaute family member, Eif2c2 (Ago2), is essential for development and appears not to be involved in DNA methylation. Genomics *89*, 687–696.

Morrisey, E.E., Tang, Z., Sigrist, K., Lu, M.M., Jiang, F., Ip, H.S., and Parmacek, M.S. (1998). GATA6 regulates HNF4 and is required for differentiation of visceral endoderm in the mouse embryo. Genes Dev. *12*, 3579–3590.

Niakan, K.K., Ji, H., Maehr, R., Vokes, S.A., Rodolfa, K.T., Sherwood, R.I., Yamaki, M., Dimos, J.T., Chen, A.E., Melton, D.A., et al. (2010). Sox17 promotes differentiation in mouse embryonic stem cells by directly regulating extraembryonic gene expression and indirectly antagonizing self-renewal. Genes Dev. *24*, 312–326.

Niakan, K.K., Schrode, N., Cho, L.T.Y., and Hadjantonakis, A.-K. (2013). Derivation of extraembryonic endoderm stem (XEN) cells from mouse embryos and embryonic stem cells. Nat. Protoc. *8*, 1028–1041.

Nichols, J., Silva, J., Roode, M., and Smith, A. (2009). Suppression of Erk signalling promotes ground state pluripotency in the mouse embryo. Development *136*, 3215–3222.

Nishi, K., Takahashi, T., Suzawa, M., Miyakawa, T., Nagasawa, T., Ming, Y., Tanokura, M., and Ui-Tei, K. (2015). Control of the localization and function of a miRNA silencing component TNRC6A by Argonaute protein. Nucleic Acids Res. *43*, 9856–9873.

O'Carroll, D., Mecklenbrauker, I., Das, P.P., Santana, A., Koenig, U., Enright, A.J., Miska, E.A., and Tarakhovsky, A. (2007). A Slicer-independent role for Argonaute 2 in hematopoiesis and the microRNA pathway. Genes Dev. *21*, 1999–2004.

Park, S.-J., Shirahige, K., Ohsugi, M., and Nakai, K. (2015). DBTMEE: a database of transcriptome in mouse early embryos. Nucleic Acids Res. *43*, D771–D776.

Plusa, B., Piliszek, A., Frankenberg, S., Artus, J., and Hadjantonakis, A.-K. (2008). Distinct sequential cell behaviours direct primitive endoderm formation in the mouse blastocyst. Development *135*, 3081–3091.

Rossant, J., and Tam, P.P.L. (2009). Blastocyst lineage formation, early embryonic asymmetries and axis patterning in the mouse. Development *136*, 701–713.

Rugg-Gunn, P.J., Cox, B.J., Ralston, A., and Rossant, J. (2010). Distinct histone modifications in stem cell lines and tissue lineages from the early mouse embryo. Proc. Natl. Acad. Sci. USA *107*, 10783–10790.

Schraivogel, D., Schindler, S.G., Danner, J., Kremmer, E., Pfaff, J., Hannus, S., Depping, R., and Meister, G. (2015). Importin-β facilitates nuclear import of human GW proteins and balances cytoplasmic gene silencing protein levels. Nucleic Acids Res. *43*, 7447–7461.

Schrode, N., Saiz, N., Di Talia, S., and Hadjantonakis, A.K. (2014). GATA6 levels modulate primitive endoderm cell fate choice and timing in the mouse blastocyst. Dev. Cell *29*, 454–467.

Selth, L.A., Close, P., and Svejstrup, J.Q. (2011). Studying RNA-protein interactions in vivo by RNA immunoprecipitation. Methods Mol. Biol. *791*, 253–264.

Shimosato, D., Shiki, M., and Niwa, H. (2007). Extra-embryonic endoderm cells derived from ES cells induced by GATA Factors acquire the character of XEN cells. BMC Dev. Biol. *7*, 80.

Smibert, P., Yang, J.S., Azzam, G., Liu, J.-L., and Lai, E.C. (2013). Homeostatic control of Argonaute stability by microRNA availability. Nat. Struct. Mol. Biol. *20*, 789–795.

Spruce, T., Pernaute, B., Di-Gregorio, A., Cobb, B.S., Merkenschlager, M., Manzanares, M., and Rodriguez, T.A. (2010). An early developmental role for miRNAs in the maintenance of extraembryonic stem cells in the mouse embryo. Dev. Cell *19*, 207–219.

Su, H., Trombly, M.I., Chen, J., and Wang, X. (2009). Essential and overlapping functions for mammalian Argonautes in microRNA silencing. Genes Dev. *23*, 304–317.

Van Stry, M., Oguin, T.H., III, Cheloufi, S., Vogel, P., Watanabe, M., Pillai, M.R., Dash, P., Thomas, P.G., Hannon, G.J., and Bix, M. (2012). Enhanced susceptibility of Ago1/3 double-null mice to influenza a virus infection. J. Virol. *86*, 4151–4157.

Wang, D., Zhang, Z., O'Loughlin, E., Lee, T., Houel, S., O'Carroll, D., Tarakhovsky, A., Ahn, N.G., and Yi, R. (2012a). Quantitative functions of Argonaute proteins in mammalian development. Genes Dev. *26*, 693–704.

Wang, P., McKnight, K.D., Wong, D.J., Rodriguez, R.T., Sugiyama, T., Gu, X., Ghodasara, A., Qu, K., Chang, H.Y., and Kim, S.K. (2012b). A molecular signature for purified definitive endoderm guides differentiation and isolation of endoderm from mouse and human embryonic stem cells. Stem Cells Dev. *21*, 2273–2287.

Wettstein, R., Bodak, M., and Ciaudo, C. (2016). Generation of a knockout mouse embryonic stem cell line using a paired CRISPR/Cas9 genome engineering tool. Methods Mol. Biol. *1341*, 321–343.

Winter, J., and Diederichs, S. (2014). Argonaute proteins regulate microRNA stability: increased microRNA abundance by Argonaute proteins is due to microRNA stabilization. RNA Biol. *8*, 1149–1157.

Wu, J., Huang, B., Chen, H., Yin, Q., Liu, Y., Xiang, Y., Zhang, B., Liu, B., Wang, Q., Xia, W., et al. (2016). The landscape of accessible chromatin in mammalian preimplantation embryos. Nature *534*, 652–657.

Yamanaka, Y., Lanner, F., and Rossant, J. (2010). FGF signal-dependent segregation of primitive endoderm and epiblast in the mouse blastocyst. Development *137*, 715–724.

Zhao, Y., Zhao, T., Guan, J., Zhang, X., Fu, Y., Ye, J., Zhu, J., Meng, G., Ge, J., Yang, S., et al. (2015). A XEN-like state bridges somatic cells to pluripotency during chemical reprogramming. Cell *163*, 1678–1691.